PCCP

PAPER

View Article Online
View Journal | View Issue

Cite this: *Phys. Chem. Chem. Phys.*, 2016, **18**, 25893

^{35}Cl dynamic nuclear polarization solid-state NMR of active pharmaceutical ingredients†

David A. Hirsh,[a] Aaron J. Rossini,*[bc] Lyndon Emsley[d] and Robert W. Schurko*[a]

Received 21st June 2016,
Accepted 23rd August 2016

DOI: 10.1039/c6cp04353d

www.rsc.org/pccp

In this work, we show how to obtain efficient dynamic nuclear polarization (DNP) enhanced ^{35}Cl solid-state NMR (SSNMR) spectra at 9.4 T and demonstrate how they can be used to characterize the molecular-level structure of hydrochloride salts of active pharmaceutical ingredients (APIs) in both bulk and low wt% API dosage forms. ^{35}Cl SSNMR central-transition powder patterns of chloride ions are typically tens to hundreds of kHz in breadth, and most cannot be excited uniformly with high-power rectangular pulses or acquired under conditions of magic-angle spinning (MAS). Herein, we demonstrate the combination of DNP and ^{1}H–^{35}Cl broadband adiabatic inversion cross polarization (BRAIN-CP) experiments for the acquisition of high quality wideline spectra of APIs under static sample conditions, and obtain signals up to 50 times greater than in spectra acquired without the use of DNP at 100 K. We report a new protocol, called spinning-on spinning-off (SOSO) acquisition, where MAS is applied during part of the polarization delay to increase the DNP enhancements and then the MAS rotation is stopped so that a wideline ^{35}Cl NMR powder pattern free from the effects of spinning sidebands can be acquired under static conditions. This method provides an additional two-fold signal enhancement compared to DNP-enhanced SSNMR spectra acquired under purely static conditions. DNP-enhanced ^{35}Cl experiments are used to characterize APIs in bulk and dosage forms with Cl contents as low as 0.45 wt%. These results are compared to DNP-enhanced ^{1}H–^{13}C CP/MAS spectra of APIs in dosage forms, which are often hindered by interfering signals arising from the binders, fillers and other excipient materials.

1. Introduction

The identification of solid forms of active pharmaceutical ingredients (APIs) plays an important role in drug development, both in the discovery of new forms and quality control.[1–3] Each polymorph, pseudopolymorph (such as a hydrate or solvate), cocrystal, or salt of an API is uniquely patentable,[4,5] and can have substantially different physicochemical properties (stability, solubility, bioavailability *etc.*).[6–11] Undesired phases or impurities in dosage forms are potentially dangerous or costly; hence, new and innovative methods are needed for structurally characterizing APIs, both in the bulk phase and especially within solid dosage forms.

Solid APIs are commonly characterized using X-ray diffraction (powder or single-crystal), ^{1}H and ^{13}C solid-state NMR (SSNMR), thermogravimetric methods, and other spectroscopic techniques.[12–18] In many cases, these techniques provide adequate characterization of the bulk forms of APIs; however, they are often of limited use for dosage forms (especially those with low weight percentages, wt%, of the API). In particular, both pXRD patterns and ^{13}C SSNMR spectra of dosage forms often display interfering signals from the excipient (*e.g.*, binding ingredients and fillers), which obscure signals arising from the API.

Prior studies by our group[19–21] and others[22,23] have demonstrated that ^{35}Cl SSNMR is a valuable tool for characterizing the bulk and dosage forms of APIs that have been synthesized as HCl salts (excipients do not contain chloride ions, so there are no interfering signals in ^{35}Cl SSNMR spectra of dosage forms). Since ^{35}Cl is a quadrupolar nucleus (I = 3/2), its spectra are influenced by a combination of anisotropic chemical shift and quadrupolar interactions. The latter are particularly sensitive to small structural differences in the local Cl^- anion environments arising from variations in local hydrogen bonding.[19,20,24–27] As a result, each solid phase of an API produces a distinct ^{35}Cl SSNMR spectral fingerprint. Given the importance of identifying low concentrations of API phases within dosage forms (including impurities), it is crucial to improve the lower detection limit (LDL) of ^{35}Cl SSNMR experiments.

Our research group has developed pulse sequences that enable the rapid acquisition of broad ^{35}Cl SSNMR patterns (hundreds of kHz or more) with high S/N, even at moderate

[a] *Department of Chemistry and Biochemistry, University of Windsor, Windsor, ON, N9B 3P4, Canada. E-mail: rschurko@uwindsor.ca; Tel: +1-519-253-3000 ext. 3548*
[b] *Department of Chemistry, Iowa State University, Ames, IA 50011, USA. E-mail: arossini@iastate.edu; Tel: +1-515-294-8952*
[c] *US DOE Ames Laboratory, Ames, Iowa 50011, USA*
[d] *Institut des Sciences et Ingénierie Chimiques, Ecole Polytechnique Fédérale de Lausanne (EPFL), Lausanne, CH-1015, Switzerland*

† Electronic supplementary information (ESI) available. See DOI: 10.1039/c6cp04353d

field strengths (*e.g.*, 9.4 T). Unlike older methods,[28–30] these pulse sequences rely on phase-modulated frequency-swept WURST (wideband uniform-rate smooth truncation) pulses[31,32] for broadband excitation and polarization transfer. The WURST-CPMG (WCPMG)[33,34] and broadband adiabatic inversion cross-polarization (BRAIN-CP)[35] pulse sequences are used for direct (^{35}Cl) and indirect (^{1}H–^{35}Cl) broadband excitation of ^{35}Cl SSNMR spectra, respectively. The BRAIN-CP-WCPMG sequence (BCP for short) uses BRAIN-CP to transfer spin polarization from abundant nuclides (*e.g.*, ^{1}H) to dilute nuclides (*e.g.*, ^{35}Cl), and a subsequent WURST-CPMG pulse and windowed acquisition train for further signal enhancement (Fig. S1, ESI†).

Over the past few years, high-field dynamic nuclear polarization (DNP) has become a prominent method for achieving high gains in S/N for SSNMR experiments.[36–39] Recent developments in DNP NMR instrumentation (*e.g.*, high-frequency gyrotrons,[40,41] low-temperature MAS probes[42,43]), optimized radical polarizing agents,[44–48] and the availability of commercial DNP NMR spectrometers[49,50] have enabled signal increases in excess of 300, representing potential time savings by a factor of 90 000. DNP has enabled SSNMR experiments that were previously considered challenging/impossible, allowing the detailed the study of materials that were previously inaccessible to SSNMR.[51–60] Most materials are prepared for DNP experiments by using a simple incipient wetness impregnation procedure to coat the surface of the particles, or fill the porous volume with a radical polarizing agent solution.[47,61] Saturation of the EPR transitions of the radicals with microwaves results in enhanced polarization of the nuclei (most often protons) that are in close proximity to the polarizing agents.[46] In the case of micro-particulate organic solids (*e.g.*, APIs), DNP-enhanced polarization can be relayed from the surface of the particles into the interiors of the solids by ^{1}H–^{1}H spin diffusion without perturbing their macroscopic structure.[62,63] With this technique, DNP-enhanced solid-state NMR can be applied to organic solids,[63–66] pure APIs,[63,66–69] and low API wt% dosage forms.[69] These developments have enabled natural isotopic abundance ^{13}C–^{13}C, ^{1}H–^{15}N and ^{13}C–^{15}N correlation SSNMR experiments, which would be challenging or impossible without DNP.

To date, most DNP SSNMR studies have been limited to the characterization of nuclei with fairly narrow powder patterns (*i.e.*, breadths on the order of tens of kHz or less). These reports include the spectral acquisition of a variety of spin-1/2 nuclei as well as quadrupolar nuclei in highly symmetric environments (*e.g.*, ^{2}H, ^{14}N overtone, ^{17}O, ^{27}Al, and ^{51}V).[55,56,64,66,70–75] However, the enhancements afforded by DNP also make it an attractive technique for the acquisition of NMR spectra of broader patterns (*e.g.*, ^{35}Cl SSNMR) due to their inherently low S/N that largely results from the distribution of NMR signal across a wide frequency range. During the final preparation of the manuscript describing our work, Kobayashi *et al.* published one such example, in a report on DNP-enhanced ultra-wideline ^{195}Pt SSNMR.[76] One factor that hinders the acquisition of DNP-enhanced wideline spectra from stationary samples is that moderate- and fast-magic angle spinning (MAS) results in substantially higher DNP and sensitivity enhancements.[47,50,77–79] MAS rates of *ca.* 6 to 40 kHz provide DNP enhancements (ε) that are *ca.* 3 to 5 times higher than those obtained from static (*i.e.*, stationary sample) experiments.[47,50,77,78] Unfortunately, MAS experiments are not generally useful for patterns with breadths on the order of 100 kHz or more, especially for quadrupolar nuclides. First, MAS only results in partial averaging of the effects of the second-order quadrupolar interaction, and second, even very fast MAS may not result in the separation of the spinning sidebands from the isotropic centerband.[80] Matters are further complicated by the effects of first-order quadrupolar interactions and/or large chemical shift anisotropies. In many cases, MAS spectra of broad patterns are distorted and have low S/N, which prevents the accurate determination of quadrupolar and chemical shift tensor parameters.

Herein, we show that DNP can be used to enhance S/N in static wideline ^{35}Cl SSNMR patterns of APIs acquired with BCP methods. We detail a new protocol, called spinning-on spinning-off (SOSO) acquisition, for enhancing the DNP polarization under MAS and subsequently acquiring a wideline ^{35}Cl pattern under static conditions. These techniques result in DNP enhancements in ^{35}Cl SSNMR spectra of up to a factor of 110 at 100 K and B_0 = 9.4 T. We demonstrate the application of ^{35}Cl DNP SSNMR for the characterization of APIs in their bulk forms, as well as in dosage forms with Cl contents of as low as 0.45 wt%. The application of these techniques for polymorph differentiation, impurity identification, and the discovery of new solid phases are also demonstrated.

2. Methods

2.1 Sample preparation

Bulk samples of histidine hydrochloride monohydrate (**hist**), ambroxol hydrochloride (**ambr**), isoxsuprine hydrochloride (**isox**), diphenhydramine hydrochloride (**diph**), and cetirizine dihydrochloride (**ceti**), with purities ranging between 98 and 99 wt%, were purchased from Sigma-Aldrich Canada, Ltd and used without further purification (Fig. 1). A 10 mg tablet of isoxsuprine and a 25 mg tablet of Life Brand diphenhydramine obtained at local pharmacies were used as the dosage forms of **isox** and **diph**, respectively. The weight percentages of chlorine in the bulk and dosage samples are tabulated in the ESI† (Table S2). To prepare the samples for DNP SSNMR experiments, the bulk powders were ground by hand for several minutes in a mortar and pestle to reduce particle sizes, while the dosage form tablets were only lightly crushed to break the tablets into a fine powder. The samples were then impregnated[52,61] with *ca.* 15 μL of 15 mM TEKpol in 1,1,2,2-tetrachloroethane (TCE)[47] (**hist**, **ambr**, **isox**) or 1,3-dibromobutane (DBB) (**ceti**, **diph**) and packed into 3.2 mm sapphire rotors.

2.2 VT pXRD

Variable-temperature powder X-ray diffraction (pXRD) experiments were conducted using the APEX III software suite and a Bruker Photon 100 CMOS diffractometer with a graphite monochromator with CuKα (λ = 1.5406 Å). Samples were ground,

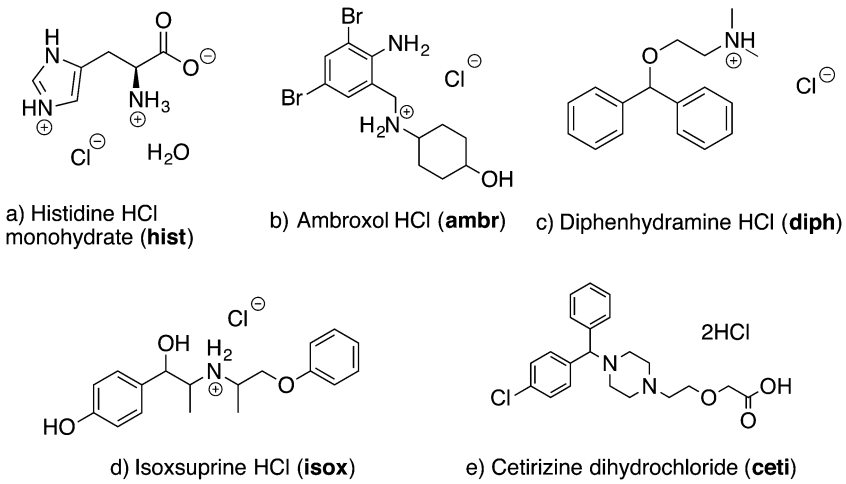

Fig. 1 Molecular structures of APIs.

packed into glass capillary tubes, and then cooled with a stream of cold N_2 from an Oxford cryostream attached to the diffractometer. pXRD patterns were acquired for all of the samples and the identities of the samples with known crystal structures were confirmed by comparison to simulated patterns (Fig. S13, ESI†).[81–84]

2.3 NMR

^{13}C and ^{35}Cl SSNMR DNP experiments were conducted on a 9.4 T (400 MHz)/263 GHz Bruker Avance III solid-state DNP NMR spectrometer[50] using a 3.2 mm HXY probe configured for ^{1}H–^{13}C–^{35}Cl experiments located at the DOE Ames Laboratory. Carbon and chlorine chemical shifts were referenced to TMS at 0 ppm, using the unified scale in the IUPAC standard.[85] Preliminary DNP NMR experiments were conducted at the EPFL (Lausanne) on a Bruker Avance I solid-state DNP NMR spectrometer equipped with a 3.2 mm HXY probe configured for ^{1}H–^{13}C–^{35}Cl.

The full experimental parameters used for the ^{13}C and ^{35}Cl experiments are given in the ESI† (Tables S3–S6). NMR-^{13}C: all ^{1}H–^{13}C CP/MAS experiments used a CP contact time of 2 ms, and a constant ^{13}C spin lock rf field of *ca.* 74 kHz. An MAS frequency of 8 kHz (or 9 kHz for **isox**) was used. The ^{1}H spin lock amplitude was linearly ramped[86–88] from *ca.* 75 kHz to 83 kHz. Proton decoupling was applied for each acquisition using an rf field of 100 kHz and the SPINAL-64 pulse sequence.[89] NMR-^{35}Cl: ^{1}H–^{35}Cl CP-CPMG and CP-echo spectra of **hist** were acquired using conventional rectangular pulses with *ca.* 70 kHz rf on both channels. The ^{1}H–^{35}Cl BRAIN-CP-WURST-CPMG (BCP) pulse sequence[35] was used to acquire the spectra of all of the other samples. The sweep direction of the WURST pulse applied during the BCP contact period can result in lopsided powder patterns; to minimize these effects on the ^{35}Cl powder patterns of **isox** and **diph**, two sub-spectra were acquired with opposite sweep directions for the BCP contact pulses. These sub-spectra were then co-added together to form the final spectrum (Fig. S11, ESI†). With the exception of the spectra of **hist**, all of the ^{35}Cl spectra were acquired using WURST-CPMG (WCPMG) refocusing pulses.[33,34] To process these spectra, the echoes in each FID were co-added to form a single echo, which was then Fourier transformed and magnitude processed.

Because of the breadth of the ^{35}Cl powder pattern of **ceti** (*vide infra*), its ^{1}H–^{35}Cl BCP spectrum was acquired using frequency-stepped acquisition.[28,29,90] Four pieces were acquired with the transmitter frequencies separated by 50 kHz increments. These pieces were then co-added together to produce the final spectrum.

The dipolar hetero-nuclear multiple-quantum correlation rotatory-resonance recoupling (D-HMQC-R_3) pulse sequence[91,92] was used to obtain a 2D dipolar ^{13}C–^{35}Cl correlation spectrum in the **hist** sample. See Table S4 for the experimental parameters (ESI†).

2.4 Software

All spectra were processed using the TopSpin 3.2 software package. Analytical simulations of the processed ^{35}Cl SSNMR spectra (Fig. S5–S9, ESI†) were generated using the Solid Lineshape Analysis module (v. 2.2.4) within TopSpin. The resulting quadrupolar and chemical shift parameters are listed in Table S7 (ESI†). Simulated ^{35}Cl MAS NMR spectra were obtained using the simulation program for solid-state NMR spectroscopy (SIMPSON).[93,94]

3. Results and discussion

3.1 Histidine HCl

Histidine HCl (**hist**) is an excellent setup standard for DNP experiments due to its long $T_1(^{1}H)$, which is *ca.* 284 s at 100 K. Slow longitudinal relaxation is advantageous for remote DNP, as it allows for increased ^{1}H polarization buildup and greater DNP enhancements.[47] The ^{1}H–^{13}C CP/MAS NMR spectra of **hist** obtained with and without microwaves are shown in Fig. 2a. The corresponding ^{13}C DNP enhancement ($\varepsilon_{CP}(^{13}C) = 260$) is the highest measured for all of the compounds in this study. All ^{13}C signals from histidine are easily resolved and differentiated from the broad 1,1,2,2-tetrachloroethane (TCE) solvent peak at *ca.* 75 ppm.

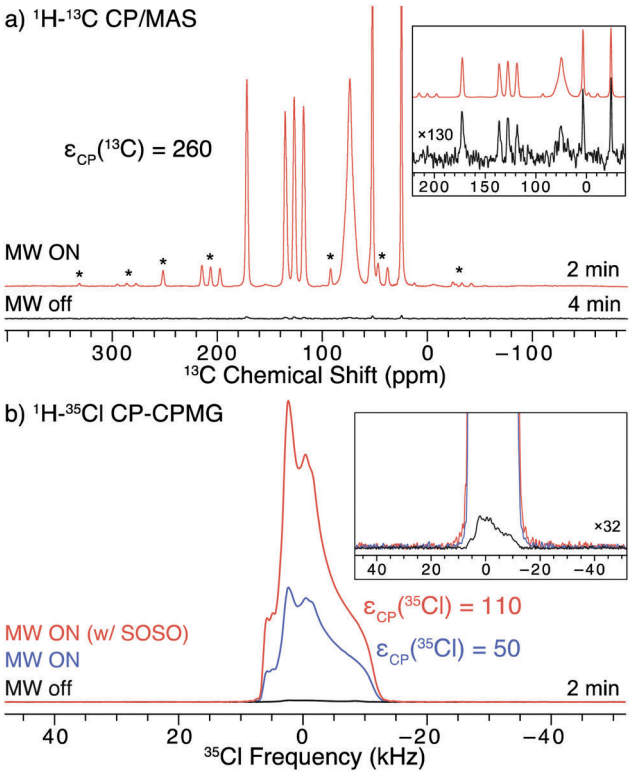

Fig. 2 ^{13}C and ^{35}Cl SSNMR spectra of finely ground **hist** impregnated with a 15 mM TEKPol/TCE solution acquired at 100 K and B_0 = 9.4 T. (a) $^{1}H-^{13}C$ CP/MAS spectra acquired with and without microwaves. The top inset shows the two ^{13}C spectra scaled to the same maximum intensity. Asterisks denote spinning sidebands. (b) $^{1}H-^{35}Cl$ CP-CPMG spectra acquired with microwaves and rotation during part of the recycle delay period (SOSO conditions, red), with microwaves and a stationary sample (blue), and a stationary sample without microwaves (black). The inset shows a vertical expansion of the ^{35}Cl SSNMR spectra.

The $^{1}H-^{35}Cl$ CP-CPMG NMR spectra of **hist** acquired with and without DNP are shown in Fig. 2b. Even under completely static sample conditions, a large DNP enhancement is observed when the microwaves are turned on ($\varepsilon_{CP}(^{35}Cl)$ = 50) (Fig. 2b). However, when the sample is rotated during part of the 30 s recycle/polarization delay, an additional 2.2-fold signal gain over the static DNP experiment is observed (Fig. 2b). We call this technique spinning-on spinning-off (SOSO). To acquire the spectrum with SOSO, we manually controlled the sample spinning at *ca.* 200 to 2000 Hz during the recycle delay and stopped the sample spinning several seconds before collecting a spectrum under static conditions (see Fig. S1 for a schematic diagram of the pulse sequence timings, ESI†). This procedure was repeated for each of the 4 to 8 scans in the experiment. SOSO allows for a larger ^{1}H polarization build-up due to improved DNP while the sample is spinning and acquisition of a distortion-free wideline spectrum under static conditions. The improved DNP enhancement with spinning is consistent with previous results that show increased DNP enhancements in $^{1}H-^{13}C$ CP/MAS NMR spectra with increasing sample spinning speeds up to *ca.* 10–15 kHz.[47,50,77,78]

In order to examine the effects of slow MAS on DNP efficiency (without the application of SOSO), a ^{35}Cl SSNMR spectrum was acquired with uninterrupted slow MAS at 250 Hz and the CP-echo pulse sequence (Fig. 3a). Slow MAS yields a central transition powder pattern that is very similar in appearance to that obtained from a corresponding experiment on a static sample (Fig. 3a and Fig. S2, ESI†). The signal in the spectrum acquired with continuous slow MAS is *ca.* 3.1 times greater than that acquired under static conditions (Fig. 3a). Thus, the DNP enhancement under continuous MAS is slightly greater than that obtained with SOSO (2.2 times, *vide supra*). The ^{35}Cl DNP enhancements in these spectra are lower than the enhancements seen in the ^{13}C NMR spectra, due in part to the slower MAS frequencies used in both the SOSO and slow MAS ^{35}Cl SSNMR experiments.

Since **hist** has a small quadrupolar coupling constant, a high-quality DNP enhanced CP-echo spectrum was also acquired at a faster MAS frequency of 8 kHz (Fig. S3, ESI†), resulting in a powder pattern free of overlapping spinning sidebands.

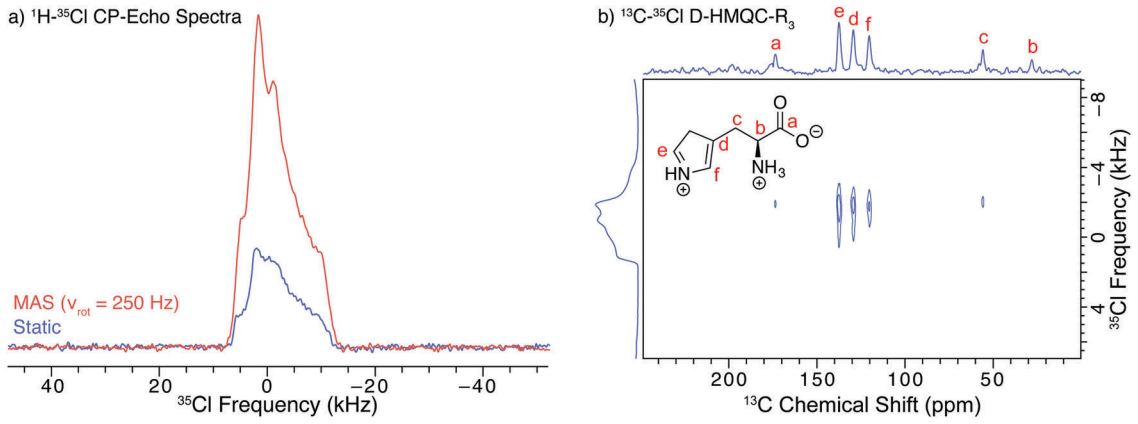

Fig. 3 (a) DNP-enhanced ^{35}Cl SSNMR spectra of finely ground **hist** impregnated with a 15 mM TEKPol/TCE solution acquired with the CP-echo pulse sequence under continuous slow MAS (ν_{rot} = 250 Hz) (red) and with the sample stationary at all times (blue). (b) 2D $^{13}C-^{35}Cl$ D-HMQC-R_3 correlation spectrum of **hist** acquired under MAS (ν_{rot} = 8 kHz) with a projection of the 2D data along the direct dimension axis and the ^{35}Cl CPMAS-echo spectrum shown along the indirect dimension axis.

The DNP enhancement of this MAS spectrum ($\varepsilon_{CP}(^{35}Cl) = 230$) is comparable to the enhancements seen in the ^{13}C NMR spectra ($\varepsilon_{CP}(^{13}C) = 260$, *vide supra*). While slow or moderate MAS experiments may be useful for acquiring spectra of narrow central transition patterns that can be partially averaged (*i.e.*, static pattern breadths <50 kHz, Fig. S3, ESI†), overlap of the MAS powder patterns with spinning sidebands is problematic for spectra with broader central transition patterns. Such overlap yields spectra without clearly defined discontinuities, which are difficult to analyze (Fig. S4, ESI† and *vide infra*). Given that the ^{35}Cl SSNMR spectra of anionic chlorides in hydrochloride salts of APIs typically have powder patterns with breadths spanning 100–300 kHz at moderate field strengths,[19–21] MAS ^{35}Cl experiments with spinning rates between 5 and 15 kHz are not suitable for the characterization of most APIs. Furthermore, the polarization transfer from ^{1}H to quadrupolar nuclei is often challenging to optimize and inefficient under MAS conditions.[95]

All of the ^{35}Cl SSNMR spectra of **hist** can be simulated with the same quadrupolar tensor parameters: C_Q = 1.8(1) MHz, η_Q = 0.72(2), δ_{iso} = 16(5) ppm (spectral simulations of these and all other ^{35}Cl powder patterns in this work can be found in the ESI:† Fig. S5–S9 and Table S7). While these parameters agree with those reported in a recent study by Pandey *et al.* (C_Q = 1.8 MHz and η_Q = 0.66),[22] they do not match those reported by Bryce *et al.* for the room temperature spectrum of **hist** (C_Q = 4.59 MHz, η_Q = 0.46, δ_{iso} = 93 ppm).[24] It is possible that the study by Bryce *et al.* involved a different polymorph of **hist**.

DNP enhancement also provides access to two-dimensional experiments that would otherwise be challenging or impossible. One such example is a 2D heteronuclear dipolar correlation spectrum of proximate ^{13}C and ^{35}Cl nuclei. As a proof of concept, we obtained a ^{13}C–^{35}Cl dipolar heteronuclear multiple-quantum correlation spectrum (Fig. 3b) with rotatory-resonance recoupling (D-HMQC-R^3).[91,92] This 2D spectrum shows correlations between the ^{13}C and ^{35}Cl nuclei that are close to each other. Such results may provide valuable distance constraints on the structure of the molecule that may be useful for NMR crystallography.[96] With DNP at higher magnetic fields and/or with faster sample spinning rates, it should be possible to acquire ^{13}C–^{35}Cl correlation spectra for APIs with larger values of C_Q. 2D ^{13}C–^{35}Cl correlation NMR spectra could enable overlapping ^{35}Cl powder patterns in APIs with multiple ^{35}Cl sites to be resolved by correlation to high resolution ^{13}C resonances.

3.2 Ambroxol HCl

Ambroxol HCl (**ambr**) is an API that is used to treat a myriad of respiratory diseases by clearing mucus from the respiratory tract. It is sold under a variety of trade names, including Mucosolvan, Mucobrox, Mucol, Lasolvan, Mucoangin, Surbronc, Ambolar, and Lysopain. A substantial DNP-enhancement ($\varepsilon_{CP}(^{13}C) = 92$) was measured for the ^{1}H–^{13}C CP/MAS NMR spectra of **ambr** (Fig. 4a). The decreased enhancement relative to **hist** could result from less favorable relaxation characteristics; the $T_1(^{1}H)$ of **ambr** at 100 K (*ca.* 30 s) is far less than that of **hist** (*ca.* 284 s), which limits the DNP enhancements of **ambr**.[62,63]

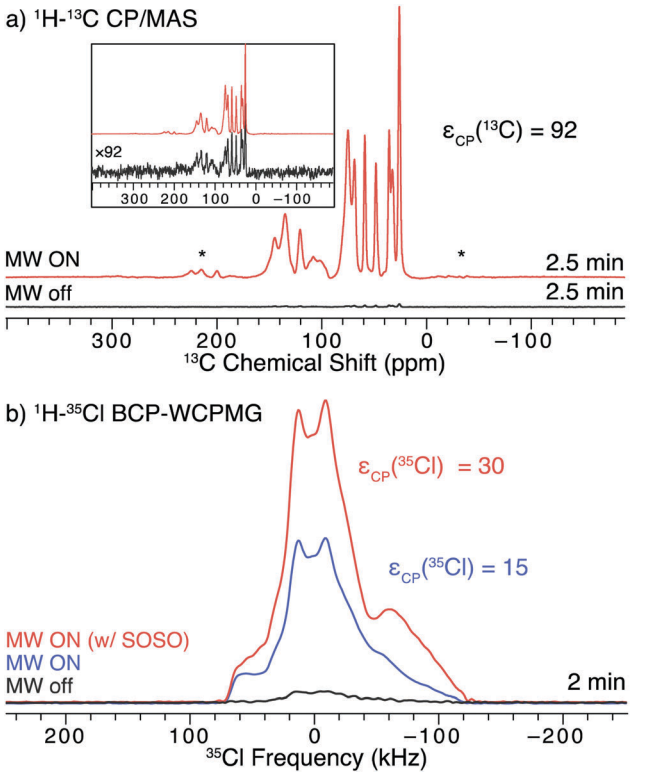

Fig. 4 ^{13}C and ^{35}Cl SSNMR spectra of finely ground **ambr** impregnated with 15 mM TEKPol/TCE solution acquired at 100 K and B_0 = 9.4 T. (a) ^{1}H–^{13}C CP/MAS spectra acquired with and without microwaves to drive DNP. The top inset shows the two ^{13}C spectra scaled to the same maximum intensity. The asterisks denote spinning sidebands. (b) ^{1}H–^{35}Cl BCP spectra acquired with microwaves and slow MAS rotation during most of recycle delay period (SOSO condition, red), with microwaves and with the sample stationary at all times (blue), and with the sample stationary without microwaves (black).

As with **hist**, DNP provides a considerable signal enhancement ($\varepsilon_{CP}(^{35}Cl) = 15$) in the ^{1}H–^{35}Cl BCP NMR spectra acquired under static conditions (Fig. 4b). If the SOSO procedure is used (*i.e.*, where the sample is spun slowly during most of the recycle delay and then is stationary during the pulse and acquisition periods), the DNP enhancement is further increased by a factor 2 and $\varepsilon_{CP}(^{35}Cl) = 30$ is observed (Fig. 4b). The combination of DNP and BCP produces a high S/N spectrum, spanning roughly 200 kHz, (*ca.* 10 times broader than that of **hist**).

Given the breadth of the ^{35}Cl powder pattern of **ambr** at 9.4 T, it is not possible to use conventional MAS (*i.e.*, constant spinning throughout the experiment). At the spinning speeds typically used for DNP-enhanced ^{13}C NMR experiments (*i.e.*, between 8 and 15 kHz), the presence of spinning sidebands distorts the ^{35}Cl pattern and makes analysis of the powder pattern challenging (Fig. S4, ESI†). These issues result because (i) slower MAS rates do not average the effects of the second-order quadrupolar interaction, leading to patterns with many overlapping sidebands that are difficult to simulate, and (ii) spinning speeds exceeding 40 to 50 kHz are necessary to separate the spinning sidebands from the isotropic centerband for typical values of ^{35}Cl C_Q at 9.4 T (or hundreds of kHz for other quadrupolar nuclides).[80]

However, DNP MAS probes with faster spinning rates have recently become available,[79] and may enable acquisition of spectra exhibiting undistorted isotropic centerbands for ^{35}Cl sites with larger values of C_Q.

There is a slight distortion in the low-frequency shoulder (at *ca.* −70 kHz) of the pattern acquired with the SOSO method. This distortion may arise from an improperly refocused CPMG echo train, which results from the sample not coming to a complete stop after spinning during the recycle delay – even very slow spinning can be disastrous for these experiments (Fig. S10, ESI†). The starting and stopping of the sample spinning was performed manually for this preliminary set of experiments. In the future, these issues could be addressed with the addition of specialized hardware to precisely control the spinning rate and stop/start timings of the sample. Alternatively, longer recycle delays could be employed, at the expense of a slight reduction in sensitivity.

3.3 Isoxsuprine HCl

The API isoxsuprine HCl (**isox**), commonly sold as Duvadilan, is a vasodilator used for both human and equine treatments. We have previously characterized **isox** in its bulk and dosage forms using ^{35}Cl static NMR experiments without DNP.[21] The ^{1}H–^{13}C CP/MAS NMR spectra of both the bulk and dosage forms of **isox** (Fig. 5a and b, respectively) can be acquired in only a few minutes with DNP ($\varepsilon_{CP}(^{13}C)$ = 86 and 32, respectively). The DNP enhancement of the signal from the API in the dosage form is much less than that from the bulk form of the API (a trend that continues with the other dosage form samples in this study, *vide infra*). Such lower DNP enhancements for dosage forms are likely due to: (i) differences in the particle sizes of the API in the bulk and dosage forms, (ii) the distribution of the radical solution in the sample, (iii) the presence of the excipient, or (iv) some combination of these factors. First, there are likely differences in the size of the API particles in the bulk and dosage forms due to the processing the API undergoes during tablet manufacturing. Second, the radical solution may be adsorbed preferentially by excipients during the impregnation step, or, if most of the API particles were coated with an excipient (*e.g.*, a polymer) during production of the dosage form, the radical solution may not penetrate the excipient.[69] Finally, the API particles may be coated with an excipient phase having an intrinsically short $T_1(^{1}H)$, a very high concentration of protons, or unfavorable dielectric properties that reduce local microwave fields. All of these effects would reduce DNP enhancements of the ^{1}H nuclei at the surface of the API particles and subsequently inside the cores of the API particles. DNP enhancements could probably be further improved on a case by case basis by optimizing the solvent used for impregnation (including investigating the use of fully- and partially-deuterated solvents), the concentration of radical in the solution, and the amount of radical solution used for the impregnation step.[62,63]

Another complication is that the DNP enhancements of signals arising from the API, solvent, and excipient molecules are not the same, as was observed in a prior study of several cetirizine dosage forms using DNP-enhanced ^{13}C SSNMR.[69]

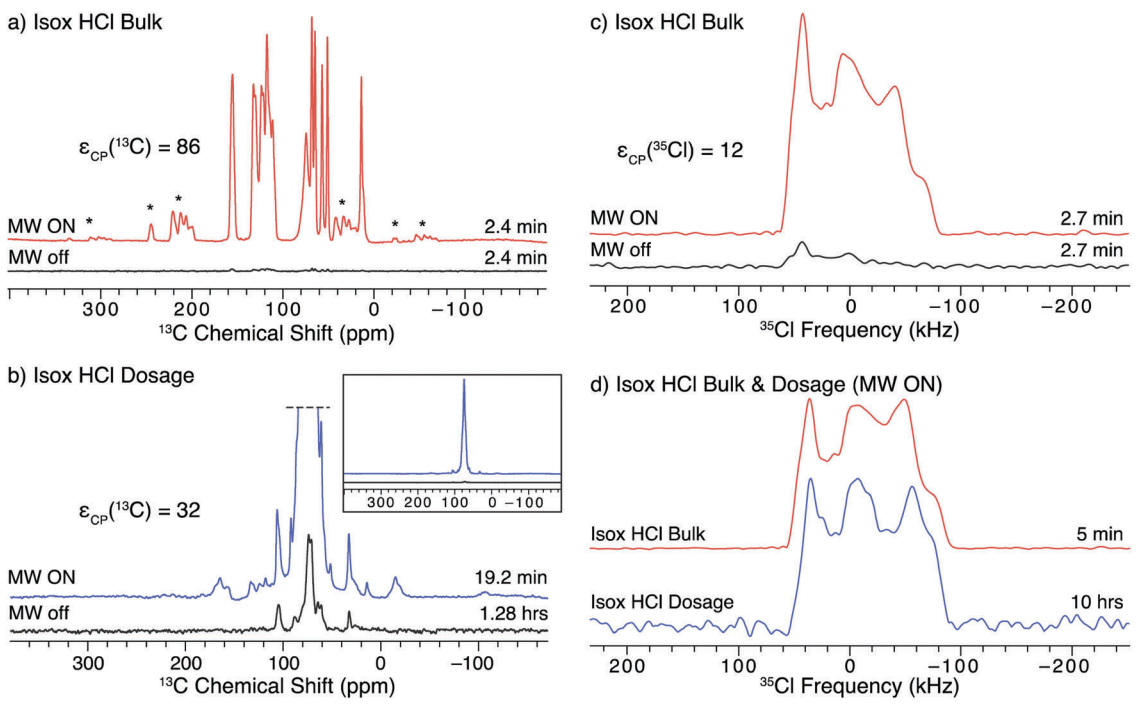

Fig. 5 SSNMR spectra of the bulk and dosage forms of **isox** impregnated with a 15 mM TEKPol/TCE solution acquired at 100 K and B_0 = 9.4 T. The left column has ^{1}H–^{13}C CP/MAS spectra of (a) the bulk API and (b) the dosage samples acquired with microwaves on and off. The bottom inset shows the full spectra of the dosage form without vertical clipping. The right column has ^{1}H–^{35}Cl BCP spectra of (c) the bulk API with and without microwaves and (d) the bulk API and dosage samples with DNP enhancement. The lineshapes in (c) are lopsided to the high frequency side because only one sweep direction of the BCP contact pulse was used (see Fig. S10 for more details, ESI†).

In the case of **isox** (Fig. 5b, inset), the strongest signal is observed for a feature at 74.8(2) ppm, which corresponds to the solvent, TCE ($\varepsilon_{CP}(^{13}C)$ = 104). This intense feature dominates the spectrum of the dosage form and obscures several peaks from the API. The DNP enhancement of the unobscured API signal (*e.g.*, peaks at *ca.* 110–135 ppm), $\varepsilon_{CP}(^{13}C)$ = 32, is less than that of the solvent. Finally, there are features that correspond to various types of excipient molecules, including polysaccharides (20–40 ppm), synthetic polymers (60–75 ppm) and stearates (100–110 ppm),[69,97,98] which have enhancements ranging from 12 to 50. Overlapping signals from the API and excipient make it challenging to determine the phase of an API in ^{13}C NMR spectra even without the use of DNP;[21] however, the differences in the DNP-enhancement such as those observed in the spectra of **isox** can further complicate the analysis. While the signal from the solvent can be decreased by adding a spin-echo to the pulse sequence[99] doing so only marginally improves the resolution of the features from **isox** (Fig. S14, ESI†).

^{35}Cl SSNMR can selectively probe the API in the dosage form without interfering signals from the excipients, since chloride ions are only found in the API and the ^{35}Cl signal from covalently-bound chlorines would be extremely broad and of too low intensity to be detected.[100–102] A comparison of the DNP-enhanced ^{1}H–^{35}Cl BCP NMR spectra of bulk and dosage forms of **isox** is shown in Fig. 5d. The DNP enhancement observed for **isox** under static conditions (Fig. 5c, $\varepsilon_{CP}(^{35}Cl)$ = 12) is comparable to that of **ambr** (*cf.* Fig. 4b). Both the ^{35}Cl SSNMR spectra of the bulk and dosage forms of **isox** are consistent with spectra acquired without DNP[19] (see Fig. S7 for the spectral simulation and associated quadrupolar parameters, ESI†). The fact that the powder pattern of the tablet matches that of the bulk compound confirms that both samples contain the same polymorph of **isox**. There are additional features in the centers of both patterns (with centers of gravity at *ca.* 0 ppm). While the origin of this feature is still under study, it may result from Cl^- anions coordinated to H_2O (*e.g.*, as a result of disproportionation of the HCl salt), or some other chemical or physical alteration of the sample (see VT-pXRD patterns in Fig. S12, ESI†).

A primary advantage of DNP experiments is that dosage forms of APIs can be studied even if the wt% of the API is very low, as is the case for **isox** (4.95 wt% API, 0.52 wt% Cl). Here, the combined acquisition time of the ^{35}Cl spectra of the pure and dosage forms of **isox** with DNP was just over 10 hours, roughly half the experiment time necessary to acquire a comparable set of spectra at room temperature.[21] Such time savings are critical in the high-throughput screening of dosage forms with low wt% APIs. Given the long acquisition times required to obtain sufficient ^{35}Cl signal without microwaves, we have not attempted to acquire these spectra, and cannot report an enhancement in the spectrum of dosage **isox** (or the other dosage forms, *vide infra*).

SOSO experiments were not conducted on **isox** because of its short $T_1(^{1}H)$ of 15 s. The short $T_1(^{1}H)$ limits the amount of time available for ^{1}H polarization build up before the polarization is lost to longitudinal relaxation. Roughly 25 s were required to start the sample spinning and completely stop rotation, which was not fast enough to fit within the optimal polarization time (20 s) for the experiments with **isox**. Of course, a longer polarization time could be applied to perform the SOSO method; however, the gains from increased DNP enhancement would be partially offset from reduced sensitivity arising from use of a recycle delay longer than 1.3 × T_1. As with **ambr** (*vide supra*), the ^{35}Cl powder pattern is too broad for conventional MAS to be used.

3.4 Diphenhydramine HCl

Diphenhydramine HCl (**diph**) is a widely used antihistamine, most commonly sold under the trade name Benadryl. The ^{1}H–^{13}C CP/MAS NMR spectra of both bulk **diph** (Fig. 6a) and the dosage form (Fig. 6b) show fair DNP enhancement ($\varepsilon_{CP}(^{13}C)$ = 25 and 16, respectively) and can be acquired in 2 minutes or less. The most intense feature in both of these spectra is a broad feature at *ca.* 50(2) ppm, which corresponds to the solvent, 1,3-dibromobutane (DBB). DBB was used for these experiments because **diph** was found to be soluble in TCE. Distinct features corresponding to the API (*e.g.*, at 128(1) ppm) can be distinguished from those of the solvent and excipient in the spectrum of the dosage form (Fig. 6b).

The DNP enhancement observed in these spectra is not as high as those observed in the spectra of the other samples (Fig. 2, 4, and 5). One contributing factor is that **diph**, like **isox**, has a relatively short $T_1(^{1}H)$ (*ca.* 18 s), which limits the build-up of enhanced polarization in the microcrystalline solid. The choice of solvent for the radical also plays an important role, as prior studies have reported decreased enhancements when using DBB rather than TCE, however, DBB was required for solubility reasons.[47,48,103] Another disadvantage of the use of DBB is that it produces a broad solvent peak in the ^{13}C SSNMR spectra, which can obscure features from the API and excipient and make confirmation of the phase and purity even more difficult. Clearly, the identification of other compatible solvents is an important future step for the further optimization of DNP experiments on APIs.

Unlike the ^{13}C spectra, the ^{1}H–^{35}Cl BCP NMR spectra of **diph** (Fig. 6d) are free from signal interference from the excipient and solvent. The breadths of the powder patterns and locations of the discontinuities are identical, which confirm that the same phase of **diph** is present in both the bulk and dosage forms. These features are also consistent with previous work done at room temperature.[21] As with the spectra of **isox**, there is an additional low-intensity feature at *ca.* −4(2) ppm that may result from disproportionation of the API. It is difficult to measure the DNP enhancement of these spectra due to the low S/N in the spectrum acquired without microwaves (Fig. 6c). The estimated minimum value of $\varepsilon_{CP}(^{35}Cl)$ = 7 was obtained by comparing the spectra after applying a Fourier transform directly to the CPMG echo train (see Fig. S15, ESI†).

Prior ^{35}Cl SSNMR studies of this compound have relied on direct excitation experiments (*e.g.*, WCPMG)[21] because attempts to use CP at room temperature were unsuccessful due to poor CP efficiency. While CP experiments are still a challenge at low temperature, they are possible with the use of DNP. Unfortunately, the variation of CP efficiency with temperature when using the

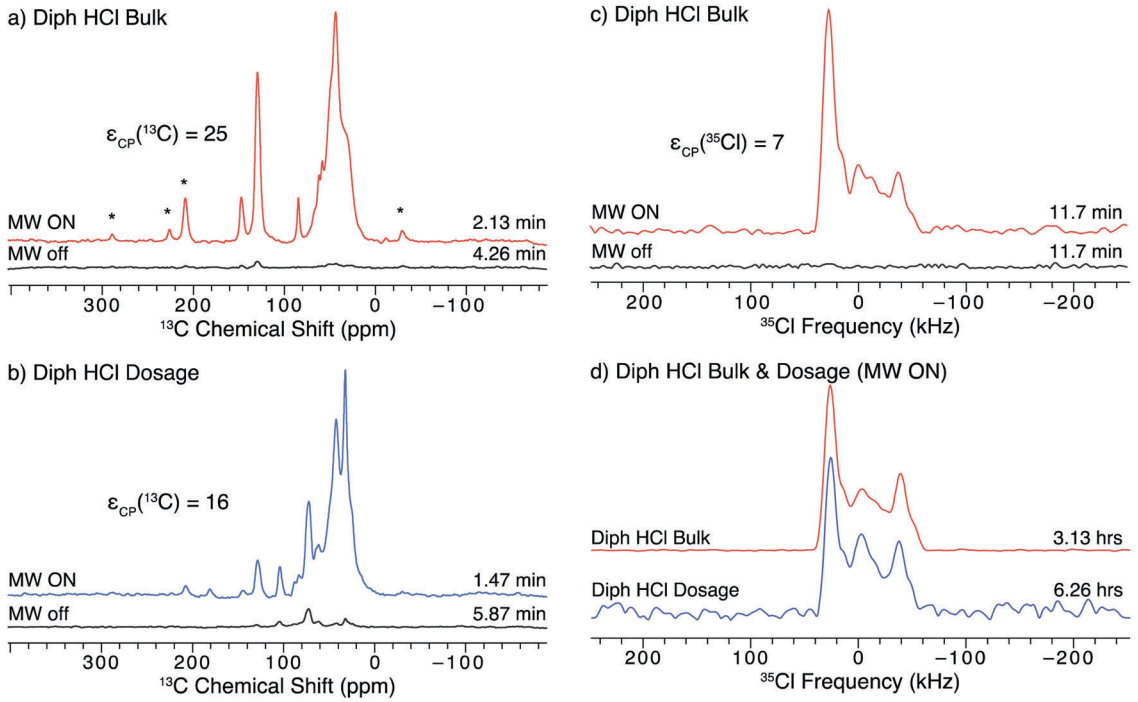

Fig. 6 ^{13}C and ^{35}Cl SSNMR spectra of the bulk and dosage forms of **diph** impregnated with a 15 mM TEKPol/1,3-dibromobutane solution acquired at 100 K and B_0 = 9.4 T. The left column has ^{1}H–^{13}C CP/MAS spectra of (a) the bulk API and (b) the dosage samples acquired with microwaves on and off. Asterisks denote spinning sidebands. The right column has ^{1}H–^{35}Cl BCP spectra of (c) the bulk API with and without microwaves and (d) the bulk API and dosage samples with DNP enhancement. The lineshape in (c) is lopsided to the high frequency side because only one sweep direction of the BCP contact pulse was used (see Fig. S10 for more details, ESI†).

BCP pulse sequence is not well understood. DNP experiments, such as those reported here, could provide opportunities for further understanding the CP dynamics, and lead to improvements to the BCP sequence and related experiments under DNP conditions.

3.5 Cetirizine HCl

SSNMR is extremely useful for the study of APIs that form solid amorphous phases.[104,105] One such API is cetirizine dihydrochloride (**ceti**), an antihistamine that is commonly sold under the trade names Zyrtec and Reactine.

The ^{1}H–^{13}C CP/MAS NMR spectra of the bulk and dosage samples of **ceti** are shown in Fig. 7a and b, respectively, and are consistent with previous studies of this compound using DNP-enhanced ^{13}C SSNMR.[69] Several distinct features from the API are apparent in the spectrum of bulk **ceti** (*e.g.*, peaks at 60–70 ppm and 130–200 ppm). However, only the strongest signal from the API (at *ca.* 130 ppm) can be distinguished in the spectrum of the dosage form due to interference from the excipients. In both spectra of **ceti**, there is less interference from the solvent than was observed in the spectra of **diph** (*cf.* Fig. 6a and b), because the DNP enhancement of the solvent peak is not as large (ε(DBB, **ceti**) = 24, ε(DBB, **diph**) = 50). The enhancement of the solvent varies from sample to sample, which may depend on the types and concentrations of different excipients, the quality of the glass formation when the radical-containing solution freezes, the amount of dissolved O_2(g), the dielectric properties of the sample that affect the microwave field,[106] or the other factors discussed above.

The enhancement observed in the spectrum of bulk **ceti** ($\varepsilon_{CP}(^{13}C)$ = 20) is close to what was previously reported for this compound ($\varepsilon_{CP}(^{13}C)$ = 31).[69] However, for **ceti** in the dosage form we measured $\varepsilon_{CP}(^{13}C)$ = 8, which is lower than the 55-fold enhancement previously reported. We attribute these decreased enhancements to the use of DBB as the radical solvent. In the previous DNP SSNMR study, **ceti** was found to be sparingly soluble in TCE.[69] We chose to use DBB (in which **ceti** is insoluble) to maximize the amount of solid sample in the rotor and to better maintain the structure of the API in the dosage form. Given that the discrepancy in enhancements is particularly apparent in the spectra of the dosage form, it is possible that DBB does not penetrate the excipients as well as TCE. Further optimization of the sample preparation could likely yield improved enhancements.

Ceti is a dihydrochloride, and its ^{35}Cl SSNMR spectra should show two distinct ^{35}Cl patterns corresponding to structurally unique Cl^- anion sites. With the use of DNP, it is possible to identify two overlapping powder patterns in the ^{35}Cl spectrum of the bulk form in just 5 minutes ($\varepsilon_{CP}(^{35}Cl)$ = 5.8, Fig. 7c). Due to hardware limitations, it is challenging to uniformly excite the entire breadth of the two ^{35}Cl patterns of **ceti**, even with BCP. As such, we used frequency-stepped acquisition[28,29] and combined 4 sub-spectra at evenly spaced transmitter frequencies to obtain the full pattern (which is *ca.* 250 kHz broad, Fig. S9, ESI†). The two overlapping ^{35}Cl powder patterns with distinct quadrupolar parameters can be readily distinguished using analytical simulations. Nonetheless, the most important discontinuities in

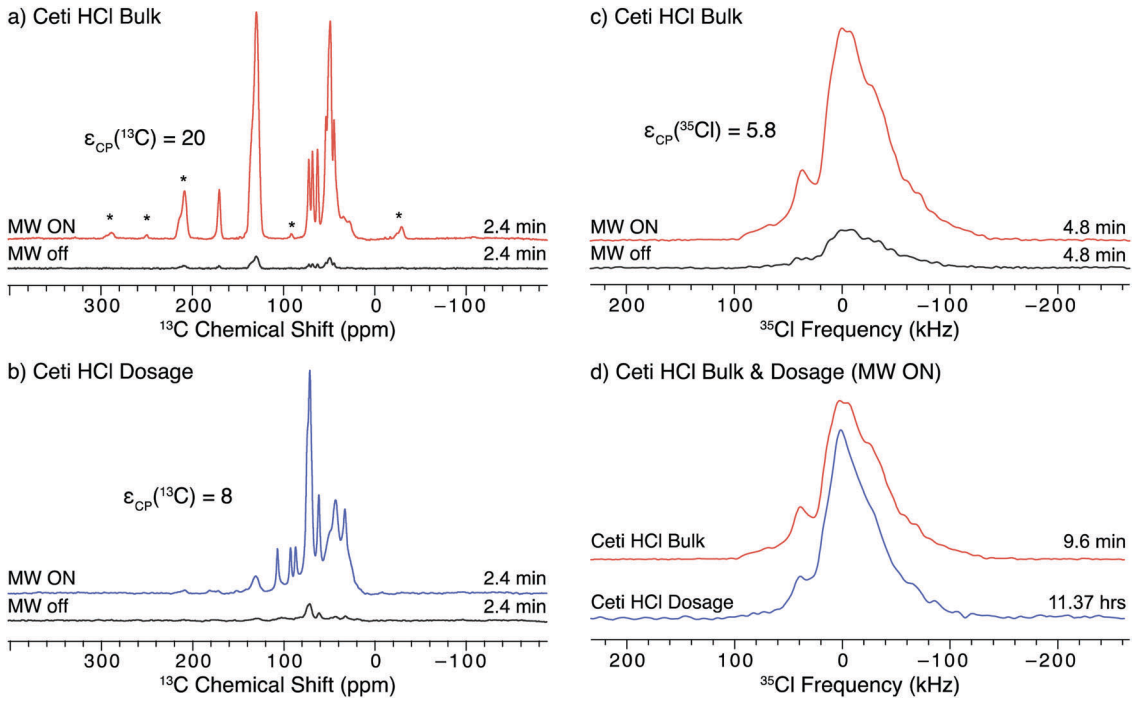

Fig. 7 ^{13}C and ^{35}Cl SSNMR spectra of the bulk and dosage forms of **ceti** impregnated with 15 mM TEKPol/1,3-dibromobutane solution acquired at 100 K and B_0 = 9.4 T. The left column has ^{1}H–^{13}C CP/MAS spectra of (a) the bulk API and (b) the dosage samples acquired with and without microwaves. Asterisks denote spinning sidebands. The right column shows the ^{1}H–^{35}Cl BCP spectra of (c) the bulk API with and without microwaves and (d) the bulk API and dosage samples with DNP enhancement.

the two patterns can be observed in the central sub-spectrum (as in Fig. 7c and d).

Acquiring a ^{35}Cl SSNMR spectrum of the dosage form with similar signal-to-noise ratio takes more than 11 hours, due to the extremely low wt% Cl in this sample (5.78 wt% API, 0.45 wt% Cl), which is the lowest discussed herein. Comparison of the ^{35}Cl spectra of the bulk and dosage forms (Fig. 7d) shows that the dosage form likely contains two ^{35}Cl environments that are similar to those of the bulk form. However, the poorer resolution of the discontinuities in the ^{35}Cl spectrum of the dosage form (most evident at the center of the pattern) is consistent with the lower crystallinity of the API within the formulation. This API was previously confirmed to exist as an amorphous form in all formulations using DNP-enhanced ^{13}C and ^{15}N SSNMR in the previous study.[69]

4. Conclusions

We have demonstrated the acquisition of high-quality static wideline ^{35}Cl SSNMR spectra of APIs using the ^{1}H–^{35}Cl BRAIN-CP-WURST-CPMG pulse sequence under DNP conditions. DNP has been observed to enhance the ^{35}Cl SSNMR signal by as much as 110 times for stationary samples. This enhancement is achieved by using a new spinning-on spinning-off (SOSO) protocol, in which the sample is spun during the recycle delay and halted shortly before the pulse/acquisition periods. The use of SOSO results in a build-up in ^{1}H polarization under MAS conditions and allows for the acquisition of a wideline ^{35}Cl spectrum free of spinning sidebands under static conditions. This method provides an additional two-fold signal enhancement over the spectra acquired with DNP under purely static conditions. The use of DNP dramatically decreases the lower detection limit for ^{35}Cl SSNMR spectra of dosage forms; we report successful characterization of APIs in bulk and dosage forms with Cl contents as low as 0.45 wt%. These ^{35}Cl NMR spectra are particularly useful for the identification of the API within the dosage form because they are not affected by interfering signals from excipient molecules in the pill. In this respect, the DNP-enhanced ^{1}H–^{13}C CP/MAS spectra of the dosage forms are limited, despite having higher signal enhancements than the corresponding ^{35}Cl NMR spectra. For all of the systems in this study, we observed lower DNP enhancements in the spectra of the dosage forms than in those of the bulk API, possibly due to the presence of excipients that reduce DNP efficiency *via* a number of different mechanisms, or due to differences in the particle size of the API in the bulk and dosage samples. These techniques show potential for investigating the sizes of micro- and nanoparticles of APIs in dosage forms.[69] Finally, we have demonstrated the use of DNP signal enhancement for the acquisition of a two-dimensional ^{13}C–^{35}Cl correlation NMR spectrum of histidine HCl monohydrate. The increasing availability of DNP MAS probes with faster spinning rates[79] will allow for the acquisition of 1D and 2D ^{35}Cl MAS NMR spectra of most chloride salts of APIs and other organic molecules, with C_Q values as high as 7 to 8 MHz at 9.4 T.

The techniques we have reported in this study will help expand the use of DNP to the study of other wideline and ultra-wideline (breadths > 250 kHz) powder patterns. While the

spectra reported herein are dominated by the second-order quadrupolar interaction, the techniques described should would work equally well for patterns that are broadened by the first-order quadrupolar interaction, chemical shift anisotropy, or combinations thereof. These developments make DNP useful for the study of a wide range of materials whose NMR spectra suffer from inherently low S/N largely due to the wide breadth of the signal.

Acknowledgements

R. W. S. acknowledges the Natural Science and Engineering Research Council (NSERC, Canada) for support in the form of Discovery, Accelerator, and Research Tools and Instruments (RTI) grants. He also acknowledges the University of Windsor for a 50th Golden Jubilee Research Chair. We are also grateful to the Canadian Foundation for Innovation (CFI), the Ontario Innovation Trust (OIT), and the University of Windsor for support of the Laboratories for Solid-State Characterization. The DNP solid-state NMR spectrometer at the Ames Laboratory was funded by US Department of Energy (DOE), Office of Science, Basic Energy Sciences, Division of Materials Science and Engineering and Division of Chemical Sciences, Geosciences, and Biosciences. The Ames Laboratory is operated for the US DOE by Iowa State University under contract no. DE-AC02-07CH11358. A. J. R. thanks the Ames Laboratory (Royalty Account) and Iowa State University for support. L. E. acknowledges the support of ERC Advanced Grant No. 320860. We thank Professors Holger Eichhorn and Jeremy Rawson (Windsor) for their assistance with the VT-pXRD measurements. We are grateful to Prof. P. Tordo, Dr O. Ouari and Dr G. Casano (Aix-Marseille Université, France) for providing the TEKPol biradical used in the DNP experiments.

References

1 F. Kesisoglou, S. Panmai and Y. Wu, *Adv. Drug Delivery Rev.*, 2007, **59**, 631–644.
2 J. Aaltonen, M. Alleso, S. Mirza, V. Koradia, K. Gordon and J. Rantanen, *Eur. J. Pharm. Biopharm.*, 2009, **71**, 23–37.
3 A. Newman, G. Knipp and G. Zografi, *J. Pharm. Sci.*, 2012, **101**, 1355–1377.
4 F. G. Vogt, *eMagRes*, John Wiley & Sons, Ltd, Chichester, UK, 2015, vol. 4, pp. 181–188.
5 A. V. Trask, *Mol. Pharmaceutics*, 2007, **4**, 301–309.
6 S. R. Chemburkar, J. Bauer, K. Deming, H. Spiwek, K. Patel, J. Morris, R. Henry, S. Spanton, W. Dziki, W. Porter, J. Quick, P. Bauer, J. Donaubauer, B. A. Narayanan, M. Soldani, D. Riley and K. McFarland, *Org. Process Res. Dev.*, 2000, **4**, 413–417.
7 M. R. Caira, *Design of Organic Solids*, 1998, **198**, 163–208.
8 J. Bauer, J. Morley, S. Spanton, F. J. J. Leusen, R. Henry, S. Hollis, W. Heitmann, A. Mannino, J. Quick and W. Dziki, *J. Pharm. Sci.*, 2006, **95**, 917–928.
9 D. Hörter and J. B. Dressman, *Adv. Drug Delivery Rev.*, 1997, **25**, 3–14.
10 Z. A. Langham, J. Booth, L. P. Hughes, G. K. Reynolds and S. A. C. Wren, *J. Pharm. Sci.*, 2012, **101**, 2798–2810.
11 L.-F. Huang and W.-Q. Tong, *Adv. Drug Delivery Rev.*, 2004, **56**, 321–334.
12 D. E. Bugay, *Adv. Drug Delivery Rev.*, 2001, **48**, 43–65.
13 S. Datta and D. J. W. Grant, *Nat. Rev. Drug Discovery*, 2004, **3**, 42–57.
14 R. K. Harris, *Analyst*, 2006, **131**, 351–373.
15 R. K. Harris, *J. Pharm. Pharmacol.*, 2007, **59**, 225–239.
16 F. G. Vogt, *New Applications of NMR in Drug Discovery and Development*, 2013, pp. 43–100.
17 G. A. Monti, A. K. Chattah and Y. G. Linck, *Annu. Rep. NMR Spectrosc.*, Elsevier Ltd, 2014, vol. 83, pp. 221–269.
18 F. G. Vogt, *eMagRes*, 2015, **4**, 255–268.
19 M. P. Hildebrand, H. Hamaed, A. M. Namespetra, J. M. Donohue, R. Fu, I. Hung, Z. Gan and R. W. Schurko, *CrystEngComm*, 2014, **16**, 7334–7356.
20 H. Hamaed, J. M. Pawlowski, B. F. T. Cooper, R. Fu, S. H. Eichhorn and R. W. Schurko, *J. Am. Chem. Soc.*, 2008, **130**, 11056–11065.
21 A. M. Namespetra, D. A. Hirsh, M. P. Hildebrand, A. R. Sandre, H. Hamaed, J. M. Rawson and R. W. Schurko, *CrystEngComm*, 2016, **18**, 6213–6232.
22 M. K. Pandey, H. Kato, Y. Ishii and Y. Nishiyama, *Phys. Chem. Chem. Phys.*, 2016, **18**, 6209–6216.
23 F. G. Vogt, G. R. Williams, M. Strohmeier, M. N. Johnson and R. C. B. Copley, *J. Phys. Chem. B*, 2014, **118**, 10266–10284.
24 D. L. Bryce and G. D. Sward, *J. Phys. Chem. B*, 2006, **110**, 26461–26470.
25 B. J. Butler, J. M. Hook and J. B. Harper, *Recent Advances in the NMR Spectroscopy of Chlorine, Bromine and Iodine*, Elsevier Ltd, 2011, vol. 73.
26 C. M. Widdifield, R. P. Chapman and D. L. Bryce, *Annu. Rep. NMR Spectrosc.*, Elsevier Ltd, 2009, vol. 66, pp. 195–326.
27 D. L. Bryce and E. B. Bultz, *Chem. – Eur. J.*, 2007, **13**, 4786–4796.
28 W. G. Clark, M. E. Hanson, F. Lefloch and P. Segransan, *Rev. Sci. Instrum.*, 1995, **66**, 2453–2464.
29 D. Massiot, I. Farnan, N. Gautier, D. Trumeau, A. Trokiner and J. P. Coutures, *Solid State Nucl. Magn. Reson.*, 1995, **4**, 241–248.
30 R. W. Schurko, *Acc. Chem. Res.*, 2013, **46**, 1985–1995.
31 E. Kupce and R. Freeman, *J. Magn. Reson.*, 1995, **115**, 273–276.
32 R. Bhattacharyya and L. Frydman, *J. Chem. Phys.*, 2007, **127**, 194503.
33 L. A. O'Dell, A. J. Rossini and R. W. Schurko, *Chem. Phys. Lett.*, 2009, **468**, 330–335.
34 L. A. O'Dell and R. W. Schurko, *Chem. Phys. Lett.*, 2008, **464**, 97–102.
35 K. J. Harris, A. Lupulescu, B. E. G. Lucier, L. Frydman and R. W. Schurko, *J. Magn. Reson.*, 2012, **224**, 38–47.
36 D. A. Hall, D. C. Maus, G. J. Gerfen, S. J. Inati, L. R. Becerra, F. W. Dahlquist and R. G. Griffin, *Science*, 1997, **276**, 930–932.
37 R. G. Griffin and T. F. Prisner, *Phys. Chem. Chem. Phys.*, 2010, **12**, 5737–5740.

38 T. Maly, G. T. Debelouchina, V. S. Bajaj, K.-N. Hu, C.-G. Joo, M. L. Mak-Jurkauskas, J. R. Sirigiri, P. C. A van der Wel, J. Herzfeld, R. J. Temkin and R. G. Griffin, *J. Chem. Phys.*, 2008, **128**, 052211.
39 L. R. Becerra, G. J. Gerfen, R. J. Temkin, D. J. Singel and R. G. Griffin, *Phys. Rev. Lett.*, 1993, **71**, 3561–3564.
40 L. R. Becerra, G. J. Gerfen, B. F. Bellew, J. A. Bryant, D. A. Hall, S. J. Inati, R. T. Weber, S. Un, T. F. Prisner, A. E. McDermott, K. W. Fishbein, K. E. Kreischer, R. J. Temkin, D. J. Singel and R. G. Griffin, *J. Magn. Reson.*, 1995, **117**, 28–40.
41 C. D. Joye, R. G. Griffin, M. K. Hornstein, K.-N. Hu, K. E. Kreischer, M. Rosay, M. A. Shapiro, J. R. Sirigiri, R. J. Temkin and P. P. Woskov, *IEEE Trans. Plasma Sci.*, 2006, **34**, 518–523.
42 A. B. Barnes, M. L. Mak-Jurkauskas, Y. Matsuki, V. S. Bajaj, P. C. A. van der Wel, R. DeRocher, J. Bryant, J. R. Sirigiri, R. J. Temkin, J. Lugtenburg, J. Herzfeld and R. G. Griffin, *J. Magn. Reson.*, 2009, **198**, 261–270.
43 M. Rosay, J. C. Lansing, K. C. Haddad, W. W. Bachovchin, J. Herzfeld, R. J. Temkin and R. G. Griffin, *J. Am. Chem. Soc.*, 2003, **125**, 13626–13627.
44 C. Song, K.-N. Hu, C.-G. Joo, T. M. Swager and R. G. Griffin, *J. Am. Chem. Soc.*, 2006, **128**, 11385–11390.
45 C. Sauvée, M. Rosay, G. Casano, F. Aussenac, R. T. Weber, O. Ouari and P. Tordo, *Angew. Chem., Int. Ed.*, 2013, **52**, 10858–10861.
46 K.-N. Hu, H. Yu, T. M. Swager and R. G. Griffin, *J. Am. Chem. Soc.*, 2004, **126**, 10844–10845.
47 A. Zagdoun, G. Casano, O. Ouari, M. Schwarzwälder, A. J. Rossini, F. Aussenac, M. Yulikov, G. Jeschke, C. Copéret, A. Lesage, P. Tordo and L. Emsley, *J. Am. Chem. Soc.*, 2013, **135**, 12790–12797.
48 D. J. Kubicki, G. Casano, M. Schwarzwälder, S. Abel, C. Sauvée, K. Ganesan, M. Yulikov, A. J. Rossini, G. Jeschke, C. Copéret, A. Lesage, P. Tordo, O. Ouari and L. Emsley, *Chem. Sci.*, 2016, **7**, 550–558.
49 M. Rosay, M. Blank and F. Engelke, *J. Magn. Reson.*, 2016, **264**, 88–98.
50 M. Rosay, L. Tometich, S. Pawsey, R. Bader, R. Schauwecker, M. Blank, P. M. Borchard, S. R. Cauffman, K. L. Felch, R. T. Weber, R. J. Temkin, R. G. Griffin and W. E. Maas, *Phys. Chem. Chem. Phys.*, 2010, **12**, 5850–5860.
51 T. Kobayashi, F. A. Perras, I. I. Slowing, A. D. Sadow and M. Pruski, *ACS Catal.*, 2015, **5**, 7055–7062.
52 A. J. Rossini, A. Zagdoun, M. Lelli, A. Lesage, C. Copéret and L. Emsley, *Acc. Chem. Res.*, 2013, **46**, 1942–1951.
53 O. Lafon, A. S. L. Thankamony, T. Kobayashi, D. Carnevale, V. Vitzthum, I. I. Slowing, K. Kandel, H. Vezin, J.-P. Amoureux, G. Bodenhausen and M. Pruski, *J. Phys. Chem. C*, 2013, **117**, 1375–1382.
54 W. R. Gunther, V. K. Michaelis, M. A. Caporini, R. G. Griffin and Y. Román-Leshkov, *J. Am. Chem. Soc.*, 2014, **136**, 6219–6222.
55 F. A. Perras, T. Kobayashi and M. Pruski, *J. Am. Chem. Soc.*, 2015, **137**, 8336–8339.
56 F. Blanc, L. Sperrin, D. A. Jefferson, S. Pawsey, M. Rosay and C. P. Grey, *J. Am. Chem. Soc.*, 2013, **135**, 2975–2978.
57 A. Lund, M.-F. Hsieh, T.-A. Siaw and S. Han, *Phys. Chem. Chem. Phys.*, 2015, **17**, 25449–25454.
58 H. Takahashi, D. Lee, L. Dubois, M. Bardet, S. Hediger and G. De Paëpe, *Angew. Chem., Int. Ed.*, 2012, **51**, 11766–11769.
59 D. Lee, G. Monin, N. T. Duong, I. Z. Lopez, M. Bardet, V. Mareau, L. Gonon and G. De Paëpe, *J. Am. Chem. Soc.*, 2014, **136**, 13781–13788.
60 Z. Guo, T. Kobayashi, L.-L. Wang, T. W. Goh, C. Xiao, M. A. Caporini, M. Rosay, D. D. Johnson, M. Pruski and W. Huang, *Chem. – Eur. J.*, 2014, **20**, 16308–16313.
61 A. Lesage, M. Lelli, D. Gajan, M. A. Caporini, V. Vitzthum, P. Miéville, J. G. Alauzun, A. Roussey, C. Thieuleux, A. Mehdi, G. Bodenhausen, C. Coperet and L. Emsley, *J. Am. Chem. Soc.*, 2010, **132**, 15459–15461.
62 P. C. A. van der Wel, K.-N. Hu, J. Lewandowski and R. G. Griffin, *J. Am. Chem. Soc.*, 2006, **128**, 10840–10846.
63 A. J. Rossini, A. Zagdoun, F. Hegner, M. Schwarzwälder, D. Gajan, C. Copéret, A. Lesage and L. Emsley, *J. Am. Chem. Soc.*, 2012, **134**, 16899–16908.
64 A. J. Rossini, L. Emsley and L. A. O'Dell, *Phys. Chem. Chem. Phys.*, 2014, **16**, 12890–12899.
65 K. Märker, M. Pingret, J. M. Mouesca, D. Gasparutto, S. Hediger and G. De Paëpe, *J. Am. Chem. Soc.*, 2015, **137**, 13796–13799.
66 A. J. Rossini, J. Schlagnitweit, A. Lesage and L. Emsley, *J. Magn. Reson.*, 2015, **259**, 192–198.
67 G. Mollica, M. Dekhil, F. Ziarelli, P. Thureau and S. Viel, *Angew. Chem., Int. Ed.*, 2015, **54**, 6028–6031.
68 A. C. Pinon, A. J. Rossini, C. M. Widdifield, D. Gajan and L. Emsley, *Mol. Pharmaceutics*, 2015, **12**, 4146–4153.
69 A. J. Rossini, C. M. Widdifield, A. Zagdoun, M. Lelli, M. Schwarzwälder, C. Copéret, A. Lesage and L. Emsley, *J. Am. Chem. Soc.*, 2014, **136**, 2324–2334.
70 T. Maly, L. B. Andreas, A. A. Smith and R. G. Griffin, *Phys. Chem. Chem. Phys.*, 2010, **12**, 5872–5878.
71 V. K. Michaelis, E. Markhasin, E. Daviso, J. Herzfeld and R. G. Griffin, *J. Phys. Chem. Lett.*, 2012, **3**, 2030–2034.
72 A. J. Perez Linde, D. Carnevale, P. Miéville, A. Sienkiewicz and G. Bodenhausen, *Magn. Reson. Chem.*, 2015, **53**, 88–92.
73 D. Lee, H. Takahashi, A. S. L. Thankamony, J.-P. Dacquin, M. Bardet, O. Lafon and G. De Paëpe, *J. Am. Chem. Soc.*, 2012, **134**, 18491–18494.
74 M. Valla, A. J. Rossini, M. Caillot, C. Chizallet, P. Raybaud, M. Digne, A. Chaumonnot, A. Lesage, L. Emsley, J. A. van Bokhoven and C. Copéret, *J. Am. Chem. Soc.*, 2015, **137**, 10710–10719.
75 V. Vitzthum, P. Miéville, D. Carnevale, M. A. Caporini, D. Gajan, C. Copéret, M. Lelli, A. Zagdoun, A. J. Rossini, A. Lesage, L. Emsley and G. Bodenhausen, *Chem. Commun.*, 2012, **48**, 1988–1990.
76 T. Kobayashi, F. A. Perras, T. W. Goh, T. L. Metz, W. Huang and M. Pruski, *J. Phys. Chem. Lett.*, 2016, **7**, 2322–2327.
77 K. R. Thurber and R. Tycko, *J. Chem. Phys.*, 2012, **137**, 084508.

78 F. Mentink-Vigier, Ü. Akbey, Y. Hovav, S. Vega, H. Oschkinat and A. Feintuch, *J. Magn. Reson.*, 2012, **224**, 13–21.
79 S. R. Chaudhari, P. Berruyer, D. Gajan, C. Reiter, F. Engelke, D. L. Silverio, C. Copéret, M. Lelli, A. Lesage and L. Emsley, *Phys. Chem. Chem. Phys.*, 2016, **18**, 10616–10622.
80 A. Jerschow, *Prog. Nucl. Magn. Reson. Spectrosc.*, 2005, **46**, 63–78.
81 H. Fuess, D. Hohlwein and S. A. Mason, *Acta Crystallogr., Sect. B: Struct. Crystallogr. Cryst. Chem.*, 1977, **33**, 654–659.
82 D. Schollmeyer and M. Henk, *CCDC 189162: Private communication to the Cambridge Structural Database*, 2002, DOI: 10.5517/cc6bv0c.
83 H. S. Yathirajan, B. Nagaraj, R. S. Narasegowda, P. Nagaraja and M. Bolte, *Acta Crystallogr., Sect. E: Struct. Rep. Online*, 2004, **60**, o2228–o2229.
84 R. Glaser and K. Maartmann-Moe, *J. Chem. Soc., Perkin Trans. 1*, 1990, 1205–1210.
85 R. K. Harris, E. D. Becker, S. M. Cabral de Menezes, R. Goodfellow and P. Granger, *Pure Appl. Chem.*, 2001, **73**, 1795–1818.
86 O. Peersen, X. Wu and S. Smith, *J. Magn. Reson.*, 1994, **106**, 127–131.
87 O. Peersen, X. Wu, I. Kustanovich and S. O. Smith, *J. Magn. Reson.*, 1993, **104**, 334–339.
88 G. Metz, X. L. Wu and S. O. Smith, *J. Magn. Reson.*, 1994, **110**, 219–227.
89 B. M. Fung, A. K. Khitrin and K. Ermolaev, *J. Magn. Reson.*, 2000, **142**, 97–101.
90 J. A. Tang, J. D. Masuda, T. J. Boyle and R. W. Schurko, *ChemPhysChem*, 2006, **7**, 117–130.
91 Z. Gan, J.-P. Amoureux and J. Trébosc, *Chem. Phys. Lett.*, 2007, **435**, 163–169.
92 B. Hu, J.-P. Amoureux, J. Trébosc and S. Hafner, *J. Magn. Reson.*, 2008, **192**, 8–16.
93 M. Bak, J. T. Rasmussen and N. C. Nielsen, *J. Magn. Reson.*, 2000, **147**, 296–330.
94 Z. Tošner, R. Andersen, B. Stevensson, M. Edén, N. C. Nielsen and T. Vosegaard, *J. Magn. Reson.*, 2014, **246**, 79–93.
95 A. J. Vega, *J. Magn. Reson.*, 1992, **96**, 50–68.
96 C. Martineau, J. Senker and F. Taulelle, *Annu. Rep. NMR Spectrosc.*, 2014, vol. 82, pp. 1–57.
97 D. M. Pisklak, M. A. Zielińska-Pisklak, Ł. Szeleszczuk and I. Wawer, *J. Pharm. Biomed. Anal.*, 2016, **122**, 81–89.
98 D. M. Sperger and E. J. Munson, *AAPS PharmSciTech*, 2011, **12**, 821–833.
99 W. R. Grüning, A. J. Rossini, A. Zagdoun, D. Gajan, A. Lesage, L. Emsley and C. Copéret, *Phys. Chem. Chem. Phys.*, 2013, **15**, 13270.
100 D. L. Bryce and G. D. Sward, *Magn. Reson. Chem.*, 2006, **44**, 409–450.
101 K. E. Johnston, C. A. O'Keefe, R. M. Gauvin, J. Trébosc, L. Delevoye, J. P. Amoureux, N. Popoff, M. Taoufik, K. Oudatchin and R. W. Schurko, *Chem. – Eur. J.*, 2013, **19**, 12396–12414.
102 C. A. O'Keefe, K. E. Johnston, K. Sutter, J. Autschbach, L. Delevoye, N. Popo, M. Taou, K. Oudatchin and R. W. Schurko, *Inorg. Chem.*, 2014, **53**, 9581–9597.
103 A. Zagdoun, A. J. Rossini, D. Gajan, A. Bourdolle, O. Ouari, M. Rosay, W. E. Maas, P. Tordo, M. Lelli, L. Emsley, A. Lesage and C. Coperet, *Chem. Commun.*, 2012, **48**, 654–656.
104 M. Geppi, G. Mollica, S. Borsacchi and C. A. Veracini, *Appl. Spectrosc. Rev.*, 2008, **43**, 202–302.
105 R. T. Berendt, D. M. Sperger, E. J. Munson and P. K. Isbester, *Trends Anal. Chem.*, 2006, **25**, 977–984.
106 D. J. Kubicki, A. J. Rossini, A. Purea, A. Zagdoun, O. Ouari, P. Tordo, F. Engelke, A. Lesage and L. Emsley, *J. Am. Chem. Soc.*, 2014, **136**, 15711–15718.